

# EV Battery Charging using DAB DC-DC Converter with EPS and DPS modulations

Mridul Mishra

Dept. of Electrical Engineering  
NIT Rourkela  
Rourkela, India  
221EE4441@nitrkl.ac.in

Indrajit Sarkar

Dept. of Electrical Engineering  
NIT Rourkela  
Rourkela, India  
sarkari@nitrkl.ac.in

**Abstract**—A Dual active bridge (DAB) DC-DC converter comprises two active H-bridges interfaced by a high-frequency transformer (HFT). There are several points of interest in a DAB DC-DC converter as far as the charging application is concerned, such as bidirectional power transfer capabilities, galvanic isolation between the input and output ports, and inherent zero voltage switching (ZVS) features. The DAB DC-DC converter is extensively studied to be designed and suited for various applications, especially EV charging applications. In this work, the DAB DC-DC converter is analysed to operate in the constant current (CC) and constant voltage (CV) operating modes for EV battery charging application. The CC mode of charging is achieved using extended phase shift (EPS) modulation, and the CV mode of operation is implemented using dual phase shift (DPS) modulation techniques. The CV charging mode with DPS modulation technique is achieved using Model Predictive Control (MPC). The simulation of the DAB EV charging system is carried out in MATLAB/Simulink environment, and the observed results are discussed in detail.

**Index Terms**—Dual active bridge (DAB), extended phase shift (EPS), dual phase shift (DPS), constant current (CC), constant voltage (CV)

## I. INTRODUCTION

The DAB converter is a DC-DC converter with isolation known for its attractive features like high power density, two-way power flow capability, intrinsic ZVS potential, and the input and output ports are galvanically isolated from one another using an HFT-based high-frequency link. The topology is inherently stable [1] and is discussed in several publications for its applications in microgrid [2], EV battery charging [3] and energy reserves [4]. In [5], the description of the operation of the DAB DC-DC converter using single phase shift (SPS) modulation technique, in which the switches are operated with a constant duty cycle of 0.5 or 50%, is presented. SPS modulation technique is widely utilized for the operation of DAB converter owing to its ease of analysis and implementation. The average and the small signal model of DAB DC-DC converter are presented in [5] and in [6].

A detailed discussion on the mathematical modelling of DAB converter is discussed in [7], where the generalised average model, the reduced-order and the discrete-time model are presented. These models are derived for the operation of DAB using SPS modulation technique only. However, the SPS modulation technique has the disadvantage of the

inability to minimize the device's current stress in high-power applications. The device current stress is of prime importance in applications where the voltage conversion ratio ( $K=V_p/V_s$ ) varies or deviates from unity and hence, leading to circulation of power within the bridge and degrading the converter efficiency [8]. Therefore, the phase-shift modulation techniques are further investigated for high-power applications like EV battery charging, where the intra-bridge phase shift is also introduced in addition to the inter-bridge phase shift, thereby adding another degree of freedom. Such kind of modulation techniques are the extended phase shift (EPS) [9] and dual phase shift (DPS) [10] modulation techniques and are used in this work.

The EPS modulation-based performance analysis, along with the steady-state model for EPS control, is presented in [4]. In EPS control, an intra-bridge phase shift is introduced in the primary side H-bridge of DAB. Furthermore, the EPS modulation technique extends the soft switching region of operation and expands the control range of transmitted power with enhanced regulating flexibility. A comparative analysis of transmitted power, backflow power, and device current stress is presented in [2]. This paper illustrates the implementation of a DAB DC-DC converter-based EV battery charging system. The charging in CC mode of operation is implemented using EPS modulation technique with a conventional Proportional-Integral controller.

In DPS control, to both of DAB's H-bridges, an intra-bridge phase shift is incorporated, unlike in EPS, where it is present only on the primary side. The DPS modulation technique provides superior power transfer control, and due to two degrees of freedom, the intra-bridge and inter-bridge phase shifts, there is less reactive power flow. The provisions for the selection of intra-bridge and inter-bridge phase shift ratios for DPS modulation technique are discussed in [11]. A DAB-based battery charger using DPS modulation is presented in [12]. In the work presented in this paper, the CV charging mode is implemented using MPC. The model predictive control methodology provides accurate control by identifying the future states of the system. The converter's dynamic performance is considerably superior under MPC than the conventional PI-control [13]. The predictable model for DAB is devised using the inductor voltage.

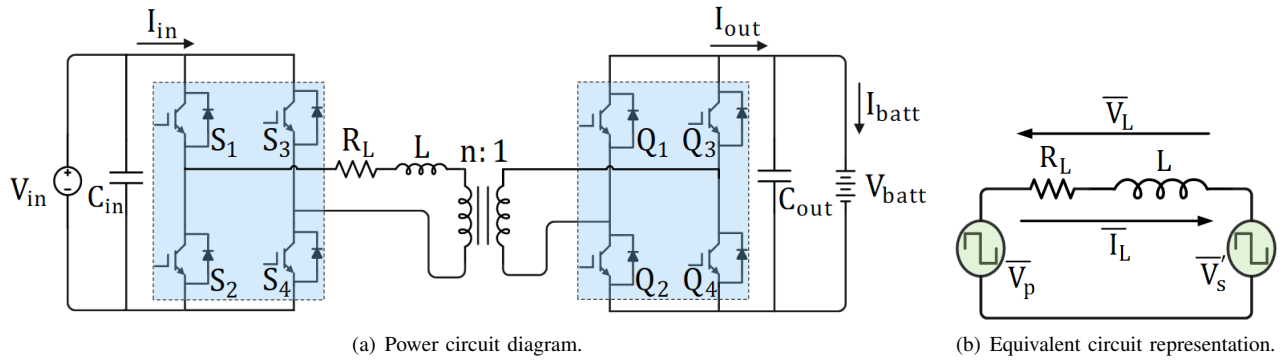


Fig. 1: The DAB DC-DC converter.

## II. DAB CONVERTER

### A. Circuit Structure

The power circuit diagram of a DAB DC-DC converter comprises two H-bridges and an HFT. The leakage inductance of the HFT is crucial for the regulated power transfer function of the DAB converter between the input and output ports. Moreover, it determines the controllable power flow range and the region for soft-switching in the converter. If a requirement arises in the design and the leakage inductance's value of the HFT is insufficient, an external inductance may be introduced to obtain the desired performance of the converter operation. Due to this, in the schematic, the leakage inductance is often shown separately, as presented in Fig.1(a). This inductor is the primary energy-storing element in the circuit which is indispensable to the converter operation. The other energy-storing elements present in the DAB system are the input and the output filter capacitors.

Two high-frequency square waves or quasi-square waves are generated across this inductor  $L$  by the two active H-bridges using the dc voltages present at the two ports of the converter. These voltages are  $V_p$ , voltage waveform generated by the primary H-bridge, and  $V_s$ , which is then transferred voltage waveform generated by the secondary H-bridge, as shown in Fig.1(b). The equivalent series resistance (ESR) is represented as  $R_L$ . The voltage across the inductor,  $V_L$ , is effectively the difference of  $V_p$  and  $V_s$  phasors. Phase-shift modulation techniques introduce phase shift among the voltages  $V_p$  and  $V_s$  to regulate the flow of current through the inductor and, by implication, the bidirectional power flow.

### B. Phase Shift Modulation Techniques for DAB Converter

The H-bridges of the DAB DC-DC converter are controlled by constant pulses of 50% duty cycle, and phase shifts are introduced in the pulses of the devices, called the intra-bridge phase shift and inter-bridge phase shift. For either of the H-bridges, the diagonal switches are switched ON and OFF simultaneously, whereas the switches in the same leg are switched in a complementary manner to avoid a dc link short circuit. The phase shift modulation techniques for DAB converter are implemented by phase shifting these switching pulses to H-bridge switches.

The inter-bridge phase shift ratio is  $D_2$  which administers the difference in phase between the switching pulses of the devices with the same subscripts in the two bridges ( $S_1$ - $Q_1$ ,  $S_4$ - $Q_4$ ) and governs the power transmission between the input and output sides, as shown in Fig. 2. It is to be noted that, in DAB converter operation, the phase leading bridge always supplies power to the phase lagging bridge [14]. In the SPS modulation, only inter-bridge phase shift is present, which controls the converter performance. However, in light load conditions SPS modulation results inferior performance as it leads to high back power flow, which in turn results in high device current stress. Such operation must be avoided as higher heat dissipation from the additional power losses will increase the size of the heat-sink and hence make the design bulky.

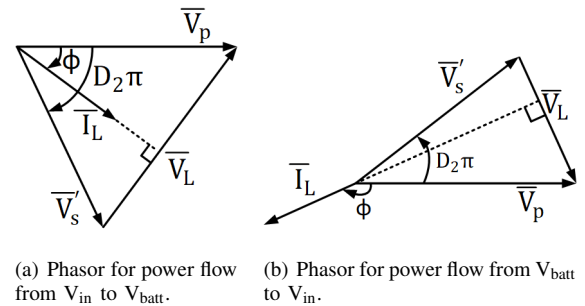


Fig. 2: Phasor representation of power flow directions.

The issues posed by the SPS modulation technique can be mitigated by using modulation techniques with intra-bridge phase shift  $D_1$  between the diagonal switches of the same H-bridge. This provides a freewheeling path for the current, and the current stress in light load conditions is significantly reduced. Modulation techniques with intra-bridge phase shifts are the EPS, DPS, and Triple Phase Shift (TPS) modulation techniques. In EPS modulation technique, the intra-bridge phase shift  $D_1$  is introduced only for the source-side H-bridge (primary side bridge), whereas in DPS modulation, this shift is present for both the H-bridge switches. It is to be noted that the intra-bridge phase shift in both the bridges is the same in case of DPS modulation, which differentiates it from TPS modulation, where the intra-bridge phase shifts of the two H-

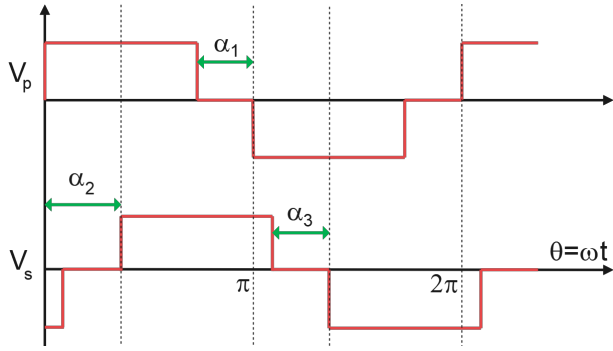


Fig. 3: Voltage waveforms produced by phase shift modulation techniques.

TABLE I: Phase shift relations

Modulation Technique	Phase Shift Angles
SPS	$\alpha_1 = \alpha_3 = 0, \alpha_2 \neq 0$
EPS	$\alpha_1 \neq 0, \alpha_3 = 0, \alpha_2 \neq 0$
DPS	$\alpha_1 = \alpha_3 \neq 0, \alpha_2 \neq 0,$
TPS	$\alpha_1 \neq \alpha_3 \neq 0, \alpha_2 \neq 0,$

bridges are different. This provides another degree of freedom while using TPS modulation technique. All the four phase shift modulation techniques are discussed in [14] along with the relevant waveforms.

The current stress issue is most prominent in SPS and is reduced in EPS, DPS and TPS modulation techniques in the mentioned order. However, the mathematical complexity invoked by the use of these techniques makes the analysis of the converter exhausting and tedious. Furthermore, the designing of the control system for the converter also becomes strenuous while using these techniques. Therefore, for analysis and modelling purposes, the SPS modulation technique is the most discussed approach. In this work, the EPS and DPS modulation techniques are used to implement the CC and CV modes for EV charging applications respectively.

### III. BATTERY CHARGING SYSTEM USING DAB CONVERTER

DC-DC converters are a critical element of the charging mechanism for EV batteries. Several DC-DC converter topologies are discussed and are found appropriate for EV battery charging applications in [15]. DAB DC-DC converter is also one of the most encouraging topologies for this application owing to its attributes like bi-directional power transfer to achieve both vehicle-to-grid (V2G) and grid-to-vehicle (G2V) modes of operations, isolation between the input and the output ports, and high power density.

Any well-designed battery charging system works in a way as to maximize the battery life and state of health (SOH) of the battery. To accomplish this, the battery charging is done in two modes, constant current (CC) charging and constant voltage (CV) charging. In CC mode of charging, the battery is charged with a constant current into the battery. This is used

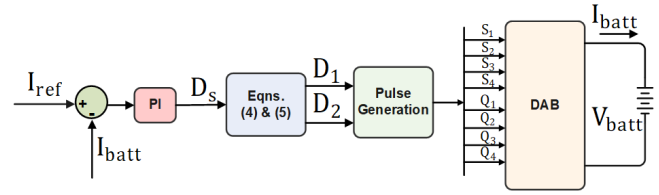


Fig. 4: Control block diagram of CC-charging mode.

for charging the battery from a low state of charge (SOC) to a certain level of SOC, which in this work is taken as the 80% of rated SOC. The CV charging mode takes control from there onwards and charges the battery at a constant terminal voltage to the voltage in fully charged condition as available in the battery's datasheet.

#### A. CC-Charging Scheme

The CC charging mode charges the battery from low SOC level to 80% SOC of the battery. In this work, this mode of operation of DAB converter is implemented using EPS modulation technique. The average DAB output current under EPS modulation is:

$$I_{out} = \frac{nV_{in}}{2f_s L} \left( D_2(1 - D_2) + \frac{D_1}{2}(1 - D_1 - 2D_2) \right) \quad (1)$$

From (1), it is visible that the average output current is dependent on both  $D_1$  &  $D_2$ . Hence, designing a PI-controller-based system would require two separate controllers as a PI-controller is a single-input single-output system. Also, for designing the controller, we would require the small-signal model of the DAB under EPS modulation. Hence, an alternative approach is considered for attaining the required design. The control system is designed for SPS modulation as with SPS modulation scheme, the average output current is a function of only one variable, the inter-bridge phase shift ratio  $D_s$ :

$$I_{out} = \frac{nV_{in}}{2f_s L} D_s (1 - D_s) \quad (2)$$

In [6], the DAB converter modelling is presented for bi-directional battery charging using SPS modulation. Perturbing and linearizing (2), we get the small-signal equation as:

$$\hat{i} = \frac{nV_{in}}{2f_s L} (1 - 2D_s) \hat{d}_s + \frac{nD_s(1 - D_s)}{2f_s L} v_{in} \quad (3)$$

Since the input dc voltage  $V_{in}$  is taken as a constant voltage source and hence, the small-signal variations in the input voltage will be zero. Therefore, the term with  $v_{in}$  in (3) is eliminated. Using these dynamics, the PI controller is designed to generate the  $D_s$ . Then based on current stress optimization, this SPS phase shift ratio  $D_s$  is utilized to find the phase shift ratios  $D_1$  and  $D_2$  for EPS modulation as presented in [16].

The relation between these phase shift ratios, as given in [16], are:

$$D_1 = \begin{cases} \frac{1-\sqrt{2(1-2D_s)^2-1}}{2}, & K < 2, 0 \leq D_s < \left(\frac{2-\sqrt{2}}{4}\right) \\ \frac{1+\sqrt{2(1-2D_s)^2-1}}{2}, & K \geq 2, 0 \leq D_s < \left(\frac{2-\sqrt{2}}{4}\right) \\ \sqrt{2}\frac{(1-2D_s)}{2}, & K \geq 2, \left(\frac{2-\sqrt{2}}{4}\right) \leq D_s < \frac{1}{2} \end{cases} \quad (4)$$

$$D_2 = \begin{cases} 0, & 0 \leq D_s < \frac{(2-\sqrt{2})}{4} \\ \frac{(1-\sqrt{2}(1-2D_s))}{2}, & \frac{(2-\sqrt{2})}{4} \leq D_s < \frac{1}{2} \end{cases} \quad (5)$$

In EPS, there are two modes of operation which are -  $0 \leq D_1 \leq D_2 \leq 1$  and  $0 \leq D_2 \leq D_1 \leq 1$ . The difference between these modes can be observed by virtue of inductor current waveforms obtained for the two modes as presented in [17] and [18]. However, the second mode of operation, wherein  $0 \leq D_2 \leq D_1 \leq 1$ , is the more practically feasible mode of operation as  $D_1$  determines the power capability of the system and  $D_2$  controls the power flow. It is a trivial point to operate in the first mode as if primary side power is limited to a certain value due to  $D_1$ , then it becomes difficult on the secondary side to extract more power from the source. Therefore, the control scheme is designed so as to operate in  $0 \leq D_2 \leq D_1 \leq 1$  mode.

### B. CV-Charging Scheme

Once the battery is charged up to 80% SOC level with battery voltage almost at the level of a fully charged battery, the mode of charging is changed from CC to CV mode. In this charging mode, the battery is charged with a constant terminal voltage, and the current fed to the battery becomes much less than that of the CC charging mode. The main concern for controlling the DAB converter's output voltage, which was observed after going through several publications relating to this, is that a simple DC transfer function does not exist for a DAB. It appears that only the transformation action of the HFT is the factor in attaining the desired output voltage. Therefore, a detailed approach needs to be undertaken to achieve control over output port voltage. The approach undertaken here is the First Harmonic Analysis (FHA).

Referring to Fig. 1(b), we see that two high-frequency square waves or quasi-square waves are produced across the inductor  $L$ . Upon mathematically decomposing the primary side voltage  $V_p$  using the Fourier Series, we find that the RMS value of the fundamental component is directly related to  $D_1$ . Thus, by controlling the intra-bridge phase shift ratio  $D_1$ , the output voltage can be regulated. Thus, the control scheme essentially tries to maintain the  $V'_s$  phasor at a constant value by regulating  $V_p$  using  $D_1$ . However, the charging current flowing to the battery will change the battery voltage as SOC increases, so to keep  $V'_s$  constant, as shown in Fig. 5, the value of  $D_1$  needs to be regulated corresponding to the change in battery current  $I_L$ .

The Model-Predictive Control (MPC) methodology is used for CV charging mode. The prediction horizon for the predictive control is taken as one sampling instant. However, it

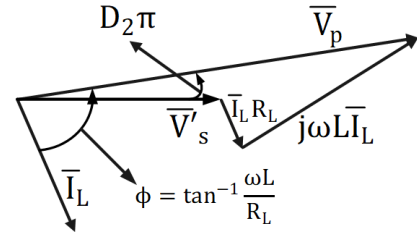


Fig. 5: Phasor diagram for voltage control mode.

can be increased as per the need. The current prediction is done using a simple Forward Euler Estimation. For the next sampling instant, the current is predicted as:

$$I_L(k+1) = I_L(k) + \frac{V_p(k) - V'_s(k)}{L f_s} \quad (6)$$

where  $V_p(k)$  and  $V'_s(k)$  are the sampled values of the primary bridge voltage and transformed secondary bridge voltage (voltage across the transformer primary), and  $f_s$  is the sampling frequency for the MPC. Now, at  $(k+1)^{\text{th}}$  instant, after the inductor current is calculated, the value of  $V_{p1}$ , RMS of  $V_p$ 's fundamental component, can be found using the phasor diagram presented in Fig. 5. The mathematical relation is obtained by resolving the components and the application of Pythagoras Theorem as:

$$V_{p1}(k+1)^2 = (V_{s1} + I_L(k+1)(R_L \cos \phi + \omega L \sin \phi))^2 + (I_L(k+1)(\omega L \cos \phi - R_L \sin \phi))^2 \quad (7)$$

After  $V_{p1}$  is obtained from (7),  $D_1$  can be calculated by the relation found using the Fourier Series decomposition of the quasi-square voltage waveform of the primary side H-bridge.  $D_2$  can be found by the application of simple trigonometric relation. Therefore, the expressions for the two phase shift ratios are:

$$D_1 = \frac{1}{2} \left[ \frac{2}{\pi} \sin^{-1} \left( \frac{V_{p1}(k+1) \pi}{V_{in} \sqrt{2}} - \frac{1}{\sqrt{2}} \right) - 1 \right] \quad (8)$$

$$D_2 = \frac{1}{\pi} \sin^{-1} \left( \frac{I_L(k+1)(\omega L \cos \phi - R_L \sin \phi)}{V_{p1}(k+1)} \right) \quad (9)$$

By using (6)-(9), a predictable model is devised and by implementing these equations, constant voltage was obtained across the battery terminals for CV mode of charging. The MPC methodology-based CV battery charging system is simulated, and the simulation results are discussed in the following section.

## IV. SIMULATION RESULTS

The DAB-based battery charging system for CC and CV modes is designed and simulated in the MATLAB/Simulink environment. The parameters for the simulation carried out are presented in Table[II].

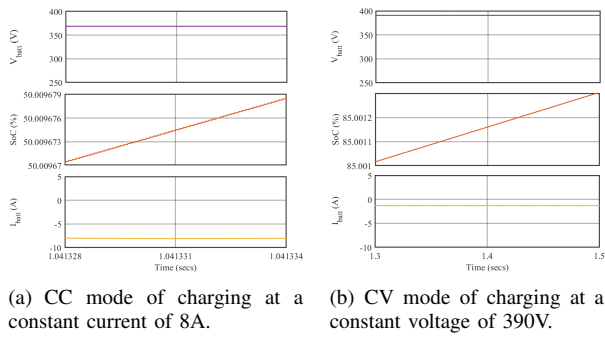


Fig. 6: Battery voltage, current and SOC.

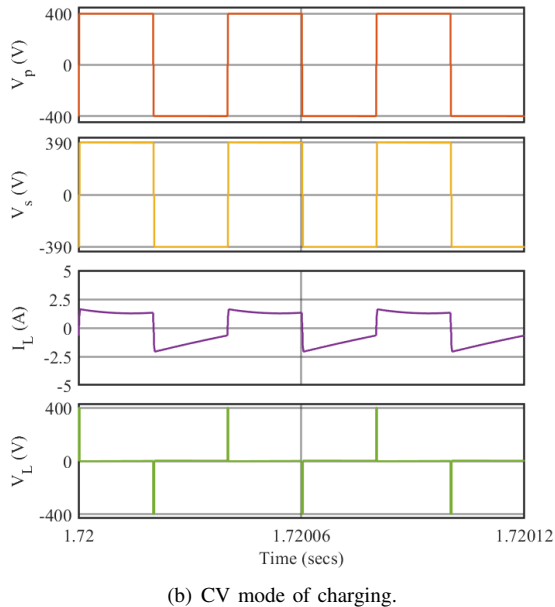
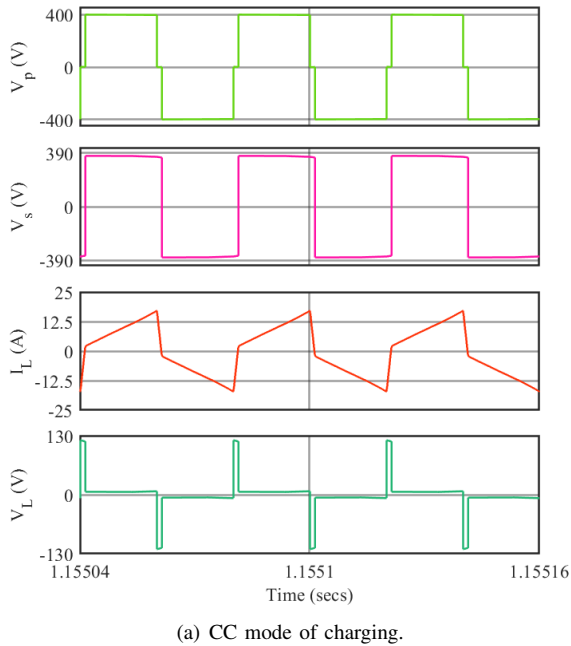


Fig. 7: Bridge voltages, inductor current and voltage.

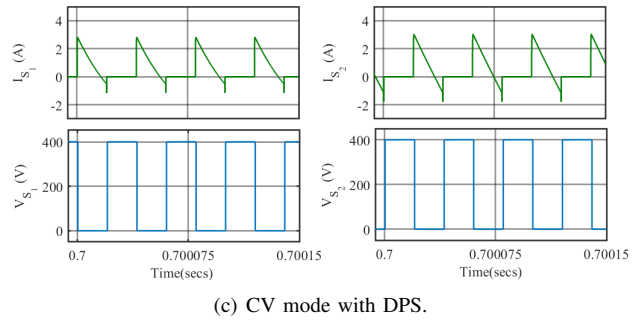
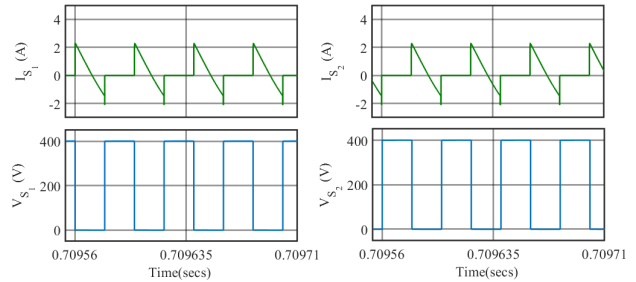
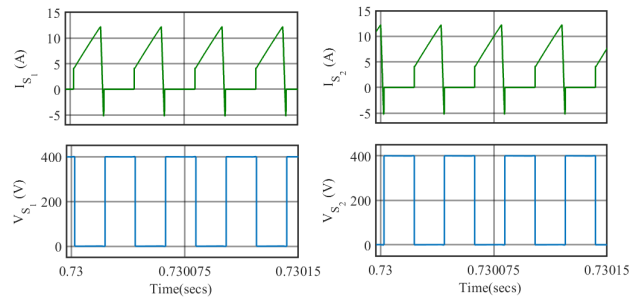


Fig. 8: Device current and voltage waveforms.

The results for the CC charging of the battery are presented in Fig. 6(a) and Fig. 7(a). The designed scheme is able to maintain constant current flowing into the battery, thereby charging it from the low level of SOC. The results for CC charging are presented for a reference current of 8 A. The bridge voltage waveforms shown in Fig. 7(a), depict the use of EPS modulation for the CC-charging scheme. The CC charging of the battery is simulated when the SOC of the battery is 50%.

Fig. 6(b) and Fig. 7(b) present the results for CV charging at a voltage level of 390V where the SOC of the battery builds up from 85% onwards. The bridge voltage waveforms presented in Fig. 7(b) show the DPS modulation used for the battery charging system. In CV charging mode, there is a slight difference between the maximum rated battery voltage and the output voltage of the battery. Therefore, the intra-bridge phase ratio  $D_1$  becomes small, and hence, the inductor voltage waveform is appearing as very narrow step pulses.

The waveforms for the voltages across the devices  $S_1$  and  $S_2$  of the DAB and the currents through them are presented

TABLE II: Simulation Parameters

Parameter	Value
Input DC Voltage( $V_{in}$ )	400 V
Nominal Battery Voltage( $V_{batt}$ )	360 V
Battery kWh Rating	9 kWh
Switching Frequency ( $f_{sw}$ )	25 kHz
Transformer VA Rating	2 kVA
Transformer Turns Ratio (n)	1.0256
Shunt Branch Parameters of the Transformer	$L_m = 720 \mu H$ , $R_c = 10 k\Omega$
Leakage Inductance (L)	42 $\mu H$
ESR of Inductance ( $R_L$ )	0.043 $\Omega$
Input Capacitor ( $C_{in}$ )	100 $\mu F$
Output Capacitor ( $C_{out}$ )	2000 $\mu F$
Sampling Time ( $T_s$ )	0.1 $\mu s$

in Fig. 8(a) for CC and Fig. 8(c) for CV charging mode. Fig. 8(c) shows the waveform of device voltage and current for CV charging mode using DPS modulation technique, and Fig. 8(b) shows the waveforms using EPS modulation technique. It is observed from the device current waveforms that there is more reverse current in the case of EPS modulation than DPS modulation for light load conditions emulated by the CV mode of charging. This justifies the selection of DPS modulation for implementing the CV charging mode as although EPS modulation scheme resulted in a good performance for CC charging mode where the reverse current in the devices is minimal, as shown in Fig. 8(a), the performance of EPS modulation deteriorates in the CV charging mode. Hence, DPS modulation scheme is employed for the CV charging mode so that the DAB DC-DC converter's optimal performance can be attained with less back-flow current.

## V. CONCLUSION

A DAB-based EV battery charging system is designed and simulated in this work which exhibits the capability and compatibility pertaining to the battery charging application for EVs. Control strategies specific to the charging mode, which are using EPS for CC mode and DPS for CV mode of charging, are presented and verified by simulation results. The EPS and DPS modulation techniques are implemented for the DAB DC-DC converter, and superior performance is observed owing to less back-flow power and current stress in the power semiconductor devices of the DAB active bridges.

## REFERENCES

[1] L. Shi, W. Lei, Z. Li, Y. Cui, J. Huang, and Y. Wang, "Stability analysis of digitally controlled dual active bridge converters," *J. Modern Power Syst. Clean Energy*, vol. 6, no. 2, pp. 375–383, 2018.

[2] B. Zhao, Q. Yu, and W. Sun, "Extended-phase-shift control of isolated bidirectional dc-dc converter for power distribution in microgrid," *IEEE Trans. Power Electron.*, vol. 27, no. 11, pp. 4667–4680, 2012.

[3] Y. Park, S. Chakraborty, and A. Khaligh, "Dab converter for ev onboard chargers using bare-die sic mosfets and leakage-integrated planar transformer," *IEEE Trans. Transport. Electric.*, vol. 8, no. 1, pp. 209–224, 2022.

[4] R. T. Naayagi, A. J. Forsyth, and R. Shuttleworth, "Performance analysis of extended phase-shift control of dab dc-dc converter for aerospace energy storage system," in *Proc. IEEE 11th Int. Conf. on Power Electron. and Drive Syst.*, 2015, pp. 514–517.

[5] A. R. Rodríguez Alonso, J. Sebastian, D. G. Lamar, M. M. Hernando, and A. Vazquez, "An overall study of a dual active bridge for bidirectional dc/dc conversion," in *Proc. IEEE Energy Convers. Congr. and Expo.*, 2010, pp. 1129–1135.

[6] V. M. Iyer, S. Gulur, and S. Bhattacharya, "Small-signal stability assessment and active stabilization of a bidirectional battery charger," *IEEE Trans. Ind. Appl.*, vol. 55, no. 1, pp. 563–574, 2019.

[7] S. Shao, L. Chen, Z. Shan, F. Gao, H. Chen, D. Sha, and T. Dragičević, "Modeling and advanced control of dual-active-bridge dc-dc converters: A review," *IEEE Trans. Power Electron.*, vol. 37, no. 2, pp. 1524–1547, 2022.

[8] G. Chen, Z. Chen, Y. Chen, C. Feng, and X. Zhu, "Asymmetric phase-shift modulation strategy of dab converters for improved light-load efficiency," *IEEE Trans. Power Electron.*, vol. 37, no. 8, pp. 9104–9113, 2022.

[9] A. Kumar, A. H. Bhat, and P. Agarwal, "Comparative analysis of dual active bridge isolated dc to dc converter with single phase shift and extended phase shift control techniques," in *Proc. 6th Int. Conf. Comput. Appl. Electr. Eng. Recent Adv. (CERA)*, 2017, pp. 397–402.

[10] B. M. Kumar, A. Kumar, A. H. Bhat, and P. Agarwal, "Comparative study of dual active bridge isolated dc to dc converter with single phase shift and dual phase shift control techniques," in *Proc. Recent Develop. Control Autom. Power Eng. (RDCAPE)*, 2017, pp. 453–458.

[11] B. Zhao, Q. Song, and W. Liu, "Power characterization of isolated bidirectional dual-active-bridge dc-dc converter with dual-phase-shift control," *IEEE Trans. Power Electron.*, vol. 27, no. 9, pp. 4172–4176, 2012.

[12] S. Chaurasiya and B. Singh, "A load adaptive dps control for dab with reduced current stress for wide load and voltage range," in *Proc. IEEE Int. Conf. on Power Electron., Drives and Energy Syst. (PEDES)*, 2020, pp. 1–6.

[13] Q. Hou, C. Li, M. Xu, X. Cao, and Y. Liu, "Dynamic performance of dab with modelpredictive control based on double phase shifting," in *Proc. IEEE 16th Conf. Ind. Electron. Appl. (ICIEA)*, 2021, pp. 1809–1813.

[14] B. Zhao, Q. Song, W. Liu, and Y. Sun, "Overview of dual-active-bridge isolated bidirectional dc-dc converter for high-frequency-link power-conversion system," *IEEE Trans. Power Electron.*, vol. 29, no. 8, pp. 4091–4106, 2014.

[15] J. Yuan, L. Dorn-Gomba, A. D. Callegaro, J. Reimers, and A. Emadi, "A review of bidirectional on-board chargers for electric vehicles," *IEEE Access*, vol. 9, pp. 51 501–51 518, 2021.

[16] N. Hou, W. Song, Y. Zhu, X. Sun, and W. Li, "Dynamic and static performance optimization of dual active bridge dc-dc converters," *J. Modern Power Syst. Clean Energy*, vol. 6, no. 3, pp. 607–618, 2018.

[17] Z. Zhang, J. Sun, P. Wang, Z. Cai, J. Kong, X. Bai, and D. Ma, "An improved dc bias elimination strategy with extended phase shift control for dual-active-bridge dc-dc," in *Proc. Chinese Automation Congr. (CAC)*, 2019, pp. 4274–4279.

[18] G. Xu, L. Li, X. Chen, Y. Liu, Y. Sun, and M. Su, "Optimized eps control to achieve full load range zvs with seamless transition for dual active bridge converters," *IEEE Trans. Ind. Electron.*, vol. 68, no. 9, pp. 8379–8390, 2021.